

# HYDROTHERMAL SYNTHESIS AT SUPERCRITICAL CONDITIONS: EXPERIMENTS AND SIMULATION

Tadafumi Adschiri, Seiichi Takami, Mitsuo Umetsu, and Takao Tsukada

Institute of Multidisciplinary Research for Advanced Materials,  
Tohoku University,  
2-1-1 Katahira, 980-8577 Sendai, Japan

## 1. Introduction

We are developing a continuous process of hydrothermal crystallization at supercritical conditions<sup>1-11</sup>. In the proposed method, metal salt aqueous solution is mixed with high temperature water to rapidly increase the temperature of the metal salt solution and thus reduce the reactions and crystallizations during the heating up period. By using this method, we succeeded in the continuous and rapid production of nano crystals.

Recent reviews<sup>4, 8, 11</sup> summarize the specific features of supercritical fluid processes for material synthesis and processing. Several key features have been found: (i) formation of nano particles<sup>1, 4, 9-11</sup>, (ii) ability to control particle morphology to some extent with pressure and temperature<sup>2, 3</sup>, and (iii) ability to provide homogeneous reducing or oxidizing atmospheres by introducing gases or additional components ( $O_2$ ,  $H_2$ ,  $H_2O_2$ )<sup>1, 4, 7</sup>. The mechanism of nano particle formation by this method was discussed with emphasis on the solubility of the metal oxide and kinetics of the hydrothermal synthesis, both of which significantly vary around the critical point due to the change of properties of water.

The rational design of this process requires the establishment of the simulation method of this process. Recently the group of the University of Nottingham intensively studied the fluid dynamics at the mixing point of a similar type of apparatus. The simulation result suggests that the mixing regime will inevitably affect the quality and quantity of product, although it has not been applied for the supercritical state. In this study we developed a simulation method of this process, based on the fluid dynamics at supercritical conditions, kinetics, solubility estimation, nucleation, particle growth, and particle coagulation. This paper will discuss the simulation results with comparing the experimental results.

## 2. Experimental

### 2.1 Experimental apparatus

Figure 1 shows an experimental apparatus that we used for hydrothermal syntheses at supercritical conditions. A metal salt aqueous solution is prepared and fed into the apparatus in one stream. In another stream, distilled water is pressurized and then heated to a temperature that is above the temperature desired. The pressurized metal salt solution stream and the pure supercritical water stream are combined in a mixing point, which leads to rapid heating and subsequent reaction in the reactor. After the solution leaves the reactor, it is rapidly quenched and in-line filters remove larger particles. For quenching the reaction, cooling water was directly fed to the reactor. Particles formed were filtered by a membrane filter and dried in an oven at 333 K for 24 h.

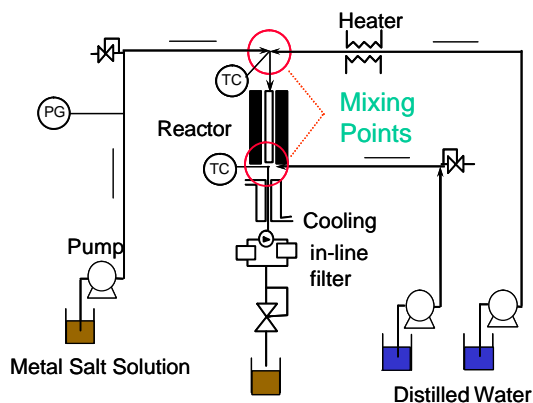


Figure 1 Experimental Apparatus

## 2.2 Metal oxide solubility

The solubility of metal oxide in high temperature water was estimated by a simplified HKF model proposed recently<sup>12,13</sup> and used for the simulation. For this calculation, Pitzer's equation<sup>12</sup> of activity coefficient was used for taking the effect of ionic strength,  $I$ , on the reaction, into account. Parameters required for the estimation were from the database for HKF model<sup>14,15</sup>. The water density was calculated by the equation of Haar *et al.*<sup>16</sup> and the dielectric constant,  $\epsilon$ , was calculated by the equation of Johnson and Norton<sup>17</sup>. The concentration of chemical species in sub- and supercritical water was calculated by solving a set of nonlinear equations (chemical equilibrium and the charge balance equation) with an iterative method. The calculated solubility was determined from the total concentration of dissolved metal species. The estimation solubility of metal oxides at the acidic conditions decreases with elevating temperature and above the critical point greatly decreased.

## 2.3 Reaction Rate

The reaction rate used for the simulation was measured experimentally by using the same apparatus shown in Figure 1 with changing length of the reactor. The first order rate constant thus evaluated in Arrhenius plot has a clear trend that the rate constants fell on a straight line in subcritical region, but the reaction rate deviated from the straight line to higher values above the critical temperature.

## 3. Simulation

We consider a process which produces nano particles by hydrothermal synthesis in supercritical phase, where the reactants and the hot water are mixed in the reactor shown in Figure 1 and consequently nano particles precipitate through chemical reaction, nucleation and crystal growth processes. Therefore, the mathematical model of the process needs to link the kinetics of chemical reaction, nucleation and crystal growth to the thermo-fluid dynamics in a wide range of temperature below and above the critical point, at which the thermophysical properties such as density change very significantly.

### 3.1 Thermo-fluid Dynamics Model

In the present work, the computational fluid dynamics program of supercritical fluid named JSTSTAR in ACT-JST Software Library was employed to calculate the flow and thermal fields in the reactor. In the JSTSTAR code, the following continuity equation, momentum equation, equation of state and energy equation are solved by the CIP method<sup>18</sup>.

$$\frac{\partial \mathbf{r}}{\partial t} + \mathbf{v} \cdot \nabla \mathbf{r} = -\mathbf{r}(\nabla \cdot \mathbf{v}) \quad (1)$$

$$\frac{\partial \mathbf{v}}{\partial t} + \mathbf{v} \cdot (\nabla \mathbf{v}) = -\frac{1}{\mathbf{r}} \nabla p + \nabla \cdot \mathbf{m} (\nabla \mathbf{v} + \nabla \mathbf{v}^T) \quad (2)$$

$$(\nabla \cdot \mathbf{v}) = -\frac{1}{\mathbf{r}c^2} \frac{dp}{dt} + \left( \frac{\partial p}{\partial T} \right)_r \frac{1}{\mathbf{r}^2 c^2 C_v} (Q - \nabla \cdot \mathbf{j}_Q) \quad (3)$$

$$\frac{\partial h}{\partial t} + \mathbf{v} \cdot \nabla h = -\frac{1}{\mathbf{r}} (\nabla \cdot \mathbf{j}_Q) \quad (4)$$

where  $\mathbf{r}$  is density,  $t$  is time,  $\mathbf{v}$  is velocity vector,  $p$  is pressure,  $\mathbf{m}$  is viscosity,  $c$  is sound speed,  $T$  is temperature,  $C_v$  is specific heat,  $Q$  is heat generation rate,  $\mathbf{j}_Q$  is heat flux and  $h$  is enthalpy. The thermophysical properties in Eqs. (1)–(4) were estimated using the steam table, assuming that the solution properties are almost the same as those of pure water because of small amount of solutes.

### 3.2 Precipitation Model

The size distribution of the particles precipitated and transported by the flow is characterized by the momentum equations<sup>19-22</sup>. The moments of the distribution represent the average or total

properties of the solid phase and can be used to calculate properties such as the total number concentration, total volume concentration and average particle volume. The moment transformation of the population balance gives the following kinetic expressions of  $j$ -th moment,  $\mathbf{m}_j$ .

$$\frac{\partial \mathbf{m}_j}{\partial t} + \mathbf{v} \cdot \nabla \mathbf{m}_j = J V_c^j + j G \mathbf{m}_{j-1} + \int_0^\infty \int_0^\infty \left( \frac{1}{2} (v+u)^j - v^j \right) \mathbf{b}(v,u) n(u) n(v) du dv \quad (5)$$

where  $J$  is the nucleation rate of particles with the critical volume  $V_c$  based on the classical primary nucleation theory, and  $G$  is the overall growth rate. The last term in Eq.(5) represents the agglomeration of two particles of volumes  $u$  and  $v-u$  into a particle of volume  $v$ , where  $\mathbf{b}$  is the aggregation kernel.

In addition, the local concentrations of the reacting species, given by the following transport equation, is needed to calculate the supersaturation, nucleation rate and the crystal growth rate.

$$\frac{\partial C}{\partial t} + \mathbf{v} \cdot \nabla C = D \nabla^2 C + k C_f - \frac{\mathbf{r}_c}{M_c} (J V_c + G \mathbf{m}_0) \quad (6)$$

where  $C$  and  $C_f$  are concentrations of product and reactant, respectively,  $D$  is diffusivity,  $k$  is reaction rate constant,  $\mathbf{r}_c$  is density of particle, and  $M_c$  is molecular weight.

Finally, by solving the coupled concentration and moments transport equations, Eqs.(5) and (6), being based on the flow and thermal fields by thermo-fluid dynamics analysis, the local concentration, supersaturation and distribution moments fields in the reactor are obtained. Here, the first 3 moments are solved, and the finite difference method based on the control volume method was used as a numerical procedure.

#### 4. Results and Discussion

In this study, we performed experiments using two types of junctions as shown in Figure 2. The mean size of generated particles for Figure 2b was smaller and the particle size distribution was narrower than those of Figure 2a. In order to elucidate the reason, we simulated the thermo-fluid dynamics inside the reactors. Figure 3 shows the calculated temperature distributions in the reactor with width of  $2.5 \times 10^{-3}$  m, where the inlet velocity of reactant at 293 K is 0.1 m/s and the hot water at 700K is 0.4 m/s. The reactant and hot water through both side streams are mixed at the tee-junction, and the temperature of the reactant increases rapidly after mixing.

Figure 4 shows the distributions of the product concentration  $C$ , the total number concentration  $n_T$  and the total volume concentration  $V_T$  of particles in two types of reactors, where the stream of reactant is oriented at 90 degree to the hot water stream in (b). After mixing, the products are consumed due to the nucleation and crystal growth. However, the nucleation completes after about 1 cm from the tee-junction, although the crystal growth continues slightly. The average particle sizes estimated by  $V_T/n_T$  at  $z = 0.12$  m are 23.8 nm and 20.2 nm in (a) and (b), respectively. Comparing between the results in (a) and (b), it is found that the particle properties depend on the way the reactants are mixed. This result agrees well with the experimental results that the shape of junction affected the size and distribution of particles and indicates that a combination of the thermo-fluid model and the solubility

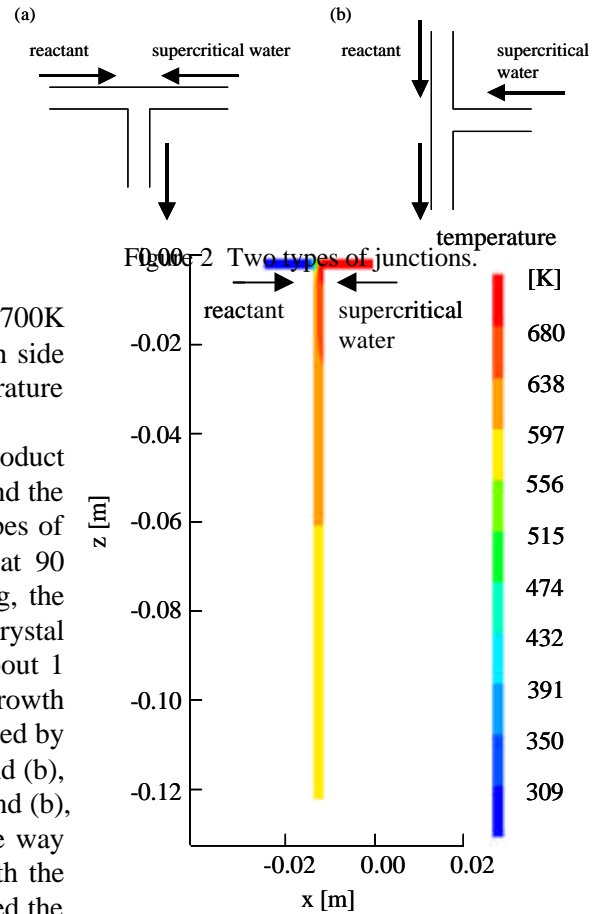


Figure 3 Temperature distribution in the reactor.

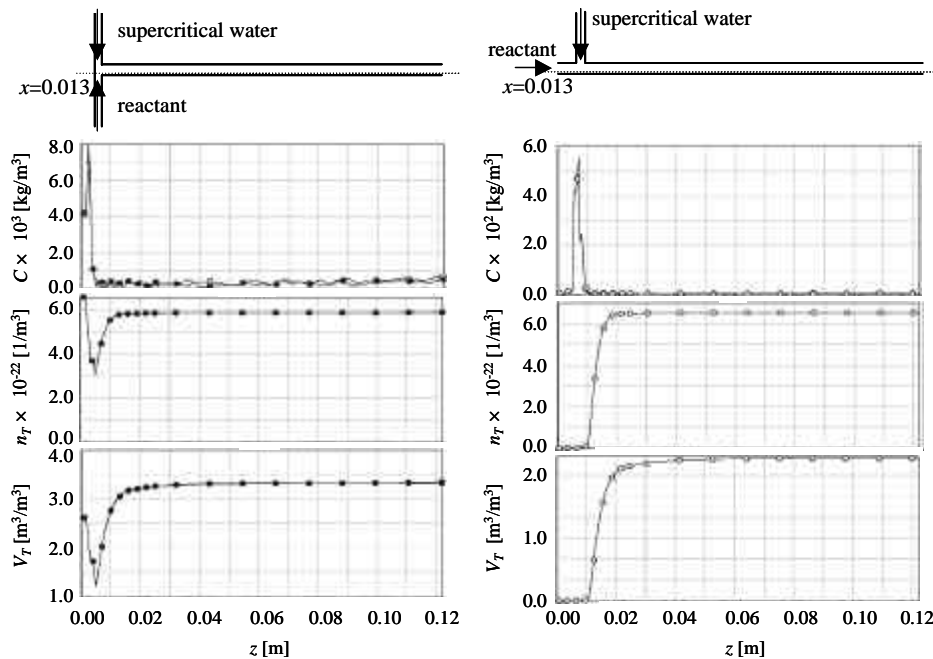


Figure 4 Product concentration ( $C$ ), the total number concentration ( $n_T$ ), and the total volume concentration ( $V_T$ ) in the reactor.

model of metal oxide enables us to design reactors rationally for hydrothermal synthesis under supercritical conditions.

### Acknowledgements

This study is carried out as a part of “Ground-based Research Announcement for Space Utilization” promoted by Japan Space Forum. The authors also wish to acknowledge the Ministry of Education, Science, Sports and Culture, Japan, Genesis Research Institute, and New Energy and Industrial Technology Organization (NEDO) for financial support of this research.

### References

- 1) T. Adschiri, K. Kanazawa, and K. Arai, *J. Am. Ceram. Soc.* **75**, 1019-1024, 1992.
- 2) T. Adschiri, K. Kanazawa, and K. Arai, *J. Am. Ceram. Soc.* **75**, 2615-2620, 1992.
- 3) Y. Hakuta, T. Adschiri, H. Hirakoso, and K. Arai, *Fluid Phase Equilib.* **158-160**, 733-739, 1999.
- 4) T. Adschiri, Y. Hakuta, and K. Arai, *Ind. Eng. Chem. Res.*, **39(12)**, 4901-4907, 2000.
- 5) Y. Hakuta, T. Adschiri, T. Suzuki, K. Seino, and K. Arai, *J. Am. Ceram. Soc.* **81(9)**, 2461-2465, 1998.
- 6) Y. Hakuta, K. Seino, H. Ura, T. Adschiri, H. Takizawa, and K. Arai, *J. Mater. Chem.* **9(10)**, 2671-2675, 1999.
- 7) T. Adschiri, Y. Hakuta, K. Kanamura, and K. Arai, *J. High Pressure Sci.*, in press.
- 8) T. Adschiri, *Kona* **16**, 89-101, 1998.
- 9) T. Adschiri, K. Kanazawa, and K. Arai, *J. Am. Ceram. Soc.* **75**, 1019-1023, 1992.
- 10) Y. Hakuta, H. Terayama, S. Onai, T. Adschiri, and K. Arai, *J. Mater. Sci. Lett.* **17**, 1211-1213, 1998.
- 11) T. Adschiri, Y. Hakuta, K. Sue, and K. Arai, *J. Nanoparticle Res.* **3**, 227-235, 2001.
- 12) K. Sue, Y. Hakuta, R. L. Smith Jr., T. Adschiri, and K. Arai, *J. Chem. Eng. Data* **44**, 1422-1426, 1999.
- 13) K. Sue, Y. Hakuta, R. L. Smith Jr., T. Adschiri, and K. Arai, *13th International Conference on the Properties of Water and Steam*, **1**, 145- 145, 1999.
- 14) E. L. Shock, D. C. Sassani, M. Willis, and D. A. Sverjensky, *Geochim. Cosmochim. Acta* **61**, 907-950, 1997.
- 15) D. A. Sverjensky, E. L. Shock, and H. C. Helgeson, *Geochim. Cosmochim. Acta.* **61**, 1359-1412, 1997.
- 16) L. Haar, J. S. Gallagher, and G. S. Kell, “NBC/NRC Steam Tables”, Hemisphere, Washington, DC, 1984
- 17) J. W. Johnson and D. Norton, *Am. J. Sci.* **291**, 541-648, 1991.
- 18) T. Oka, K. Amano, I. Enbutsu, *Trans. JSME B.* **66**, 71, 2000.
- 19) M. L. J. van Leeuwen, O. S. L. Bruinsma, G. M. van Rosmalen, *Chem. Eng. Sci.* **51**, 2595, 1996.
- 20) H. Wei and J. Garside, *Trans. IChemE.* **75**, 219, 1997.
- 21) L. Falk and E. Schaer, *Chem. Eng. Sci.* **56**, 2445, 2001.
- 22) D. L. Marchisio, R. O. Fox, A. A. Barresi, M. Garbero, and G. Baldi, *Trans. IChemE.* **79**, 998, 2001.